




Ultra-compact SOS-based bi-metallic TM-pass polarizer

Ahmed El-Sayed Abd-Elkader¹ · Eman ELDamarawy^{2,3} ·
Mohamed Farhat O. Hameed^{4,5,6} · Salah S. A. Obayya^{2,4} 

Received: 15 September 2021 / Accepted: 22 February 2022 / Published online: 24 March 2022
© The Author(s) 2022

Abstract

Ultra-compact transverse magnetic (TM)-pass polarizer based on silicon on sapphire (SOS) platform is proposed and analysed. Low power consumption, high linearity and high speed of transmission are the major advantages of the SOS platform in different commercial applications especially in the mid infrared region. The suggested structure has bimetallic configuration of aluminium doped zinc oxide (AZO) and zirconium nitride (ZrN) to highly attenuate the quasi transverse electric (TE) mode. This is due to the coupling between the fundamental TE and the surface plasmon modes. However, the transverse magnetic mode can propagate with minimal losses. At 2.0 μm operating wavelength, the proposed TM-pass polarizer realizes 20.3 dB extinction ratio (ER) with 0.14 dB insertion loss (IL) at a device length of 3.0 μm . Therefore, the reported design has advantages of compact length, high efficiency and CMOS-compatibility.

Keywords Polarization · Silicon on sapphire (SOS) · Finite-element method · Plasmonics · Pass Polarizer

✉ Mohamed Farhat O. Hameed
mfarahat@zewailcity.edu.eg

✉ Salah S. A. Obayya
sobayya@zewailcity.edu.eg

¹ Electronics and Communications Engineering Department, Faculty of Engineering, Delta University for Science and Technology, Gamasa, Dakahlia, Egypt

² Department of Electronics and Communication Engineering, Faculty of Engineering, University of Mansoura, Mansoura 35516, Egypt

³ Department of Basic Sciences, Higher Future Institute of Engineering and Technology in Mansoura, Mansoura 51, Egypt

⁴ Centre for Photonics and Smart Materials, Zewail City of Science, Technology and Innovation, Sheikh Zayed District, 6th of October City, Giza 12588, Egypt

⁵ Department of Mathematics and Engineering Physics, Faculty of Engineering, University of Mansoura, Mansoura 35516, Egypt

⁶ Nanotechnology and Nanoelectronics Engineering Program, Zewail City of Science, Technology and Innovation, October Gardens, 6th of October City, Giza 12588, Egypt

1 Introduction

Mid infrared region (MIR) has recently attracted a great attention in many applications especially in the wavelength range from 2.0 to 20.0 μm (Schliesser et al. 2012) such as absorption spectroscopy, free space communication and thermal imaging (Lloyd 2013). The MIR range is called "molecular finger print" because it occurs in almost all chemical bonds with simple vibration signatures. The main challenge in the MIR region is the bulk size and high cost of the laser source. However, compact, affordable and tunable quantum cascade lasers have lately been commercially available. Silicon photonics platform in the MIR region has various advantages due to the silicon transparency for wavelength up to 8.0 μm . In addition, silicon photonics, in the MIR region, exhibits substantially superior nonlinear characteristics than in the near-infrared region (NIR). This is due to the two-photon absorption (TPA) that goes to zero beyond 2.0 μm . Therefore, in the MIR region, the TPA problem and the associated free carriers can be neglected (Swillam et al. 2018).

Silicon on insulator (SOI) (Abd-Elkader et al. 2019a; Kandeel et al. 2019) is the most popular silicon photonics platforms due to the high index contrast between the silicon and silicon dioxide. In this context, high field confinement can be achieved with compact device footprint. The silicon on sapphire (SOS) is an alternative to the conventional SOI platform where sapphire is used instead of buried silicon dioxide as an insulator layer. The sapphire has better transparency even for longer wavelengths than the conventional SOI. Thus, the SOS platform (Mueller and Robinson 1964) is introduced as a very interesting candidate for integrated silicon photonics (Soref and Lorenzo 1986) in the MIR region. The SOS platform is commercially available and features a strong refractive index contrast ($n = 1.7$) between the core and sapphire cladding with a large transmission window of up to 5.5 μm . Furthermore, as compared to bulk silicon, the SOS platform provides low parasitic capacitance, low power consumption, good linearity, and greater isolation, and it does not require special fabrication procedures (Zou et al. 2018).

The high-index contrast between silicon core and sapphire, on the other hand, results in a considerable optical birefringence and highly polarization-dependent devices. To solve such obstacle, there is a need for polarization handling devices (Hameed and Obayya 2011, 2014) such as polarization rotators, polarization splitters and polarizers to get polarization transparent photonic integrated circuits (PICs). The use of polarization splitters and polarization rotators is highly complicated and maximizes the system size significantly. As a result, a polarizer is mandatory to stop a polarization state and allows the propagation of the other polarized wave with minimal losses. Such a simple solution can be integrated in polarization-based devices with half power loss. Consequently, wide variety of optical polarizers has been investigated. Regarding to that, optical polarizers based on all-dielectric structures, with high ERs and minimum ILs, have been reported (Wang and Ho 2010; Guan et al. 2014; Azzam et al. 2014; Azzam and Obayya 2015; El Shamy et al. 2017). However, such waveguides usually suffer from some critical drawbacks such as complex structures with long device length and narrow bandwidth with high sensitivity to fabrication errors. The mode cutoff concept has been used to design SOI TM-pass polarizer with tapered structure (Wang and Ho 2010) with a device length of 10 μm and an ER of 26 dB. Moreover, Guan et al. (2014) have fabricated SOI TM-pass polarizer with a subwavelength grating. The fabricated device has 27 dB ER, and 0.5 dB high losses at a long device length (L_D) of 9.0 μm . In addition, a symmetrically etched silicon core was used to develop SOI TE/TM pass polarizers (Azzam et al. 2014) with low losses. At $L_D = 2.5 \mu\text{m}$, the TM- and TE- pass polarizers have ERs of 30 dB and 26 dB, respectively, and 0.4 dB relatively high

IL for the two polarizers (Azzam et al. 2014). Further, the resonance tunneling effect has been used to develop SOI TE/TM-pass polarizers (Azzam and Obayya 2015). The polarization filtering depends on the birefringence between the two polarized states of the conventional silicon wire. The TM-pass polarizer achieves 20 dB ER and 0.15 dB IL with a device length of 1.31 μm . However, the TE-pass polarizer has a device length of 1.35 μm , an IL of 0.004 dB and an ER of 18 dB. However, due to the unavoidable resonant character of such polarizers (Azzam and Obayya 2015), they can only work within a restricted bandwidth. Further, El Shamy et al., (2017) have presented wideband and easy to fabricate TE-pass and TM-pass polarizers using the SOS platform for the MIR applications. The TE-pass polarizer has an ER of 25.57 dB with high IL of 1.92 dB, while, the TM-pass polarizer has 69.77 dB ER with 1.21 dB IL. However, both structures have a long device length of 23 μm (El Shamy et al. 2017).

Recently, plasmonic materials have been used for designing highly efficient and compact polarizers. With the proper design of the plasmonic waveguide, one of the two fundamental guided modes in the silicon core can be coupled with the surface plasmon modes at the metal/dielectric interface. Therefore, only one polarized mode will propagate whereas the other polarized mode has high losses. In this respect, SOI TM-pass polarizer has been designed using plasmonic/dielectric waveguides with a device length of 10.0 μm (Alam et al. 2011). However, such hybrid design has high IL of 3.0 dB and not compatible with CMOS technology. Moreover, SOI TM-pass polarizer (Ng et al. 2012) has been introduced with a copper plasmonic material which is CMOS-compatible. Such a structure suffers from low ER of 13 dB and high IL of 1.6 dB. In addition, Bai et al. (2017) have reported a low loss and compact SOI TM-pass polarizer based on hybrid plasmonic grating. The complex polarizer (Bai et al. 2017) suffers from CMOS incompatibility with ER = 25 dB, IL = 0.088 and device length of 2.5 μm . Further, Saber et al. (2018) have used highly doped p-silicon to develop plasmonic TM-pass polarizer. This design is CMOS compatible with a long L_D of 15 μm , ER = 30.11 dB and high IL = 3.08 dB at wavelength of 1.55 μm (Saber et al. 2018).

Most of the plasmonics-based polarizers have a compact device length. However, they have a drawback of high IL because of the significant Ohmic loss of the conventional plasmonic materials. Moreover, plasmonic polarizers are commonly based on gold and silver, which are neither CMOS-compatible nor chemically stable. Therefore, alternative plasmonic materials are widely used, recently, instead of the conventional plasmonic materials. Transparent conducting oxide (TCOs) and transitional metal nitrides drew the most attention to replace conventional plasmonic materials. The new plasmonic materials have great advantages over the conventional materials such as tunability, lower losses, high design flexibility, and high compatibility with CMOS fabrication technology (Naik et al. 2011). Accordingly, TE/TM pass polarizers were presented in (Azzam and Obayya 2016) using titanium nitride material. An ER = 20 dB and IL = 0.063 dB have been achieved at $L_D = 3.5 \mu\text{m}$ for the TE-pass polarizer (Azzam and Obayya 2016). On the other hand, the TM-pass polarizer realized ER = 20 dB and IL = 0.96 dB at $L_D = 2.84 \mu\text{m}$. Additionally, ultra-compact SOI TE/TM-pass polarizers were proposed in (Abd-Elkader et al. 2019b) based on AZO. An ER of 20.6 dB has been achieved with low IL of 0.21 at a compact L_D of 3.5 μm using the TE-pass polarizer. However, the TM-pass polarizer has ER = 22 dB and IL = 0.11 dB at $L_D = 1.0 \mu\text{m}$ (Abd-Elkader et al. 2019b). Further, CMOS compatible TE/TM-pass polarizers with bi-metallic configuration of indium tin oxide and zirconium nitride have been reported in (Kandeel et al. 2019). A large coupling occurs between one polarized core mode and the surface plasmon mode due to the bi-metallic configuration, while the other polarized mode can propagate with low losses. At $\lambda = 1.55 \mu\text{m}$, the TE-pass

polarizer has $ER = 32.7$ dB with IL of 0.13 dB at a compact $L_D = 1.5$ μm . In addition, the TM-pass polarizer, at $L_D = 2$ μm , has an ER of 31.5 dB and IL of 0.17 dB (Kandeel et al. 2019).

In this paper, a TM-pass polarizer based on SOS platform is introduced and analyzed for MIR applications. The proposed polarizer has a bimetallic configuration of AZO/ZrN to highly suppress the TE mode in a compact length. The AZO is one of the most attractive TCO materials because it is reasonably inexpensive and abundant element with non-toxicity. The AZO has also advantages of optical tunability, low Ohmic loss, and high thermal stability (Lin et al. 2016; Naik et al. 2013). Further, the ZrN is one of metal nitrides with favorable features such as high melting temperature state, metallic properties, optical tunability and mechanical stability. Moreover, it is compatible with silicon CMOS fabrication technology. The ZrN deposition can be achieved by many techniques like chemical vapor deposition (CVD), physical vapor deposition (PVD) or atomic layer deposition (ALD) (Naik et al. 2013). The proposed TM pass polarizer achieves 20.3 dB of ER and 0.14 dB IL with a 3.0 μm device length at a wavelength of 2.0 μm . The suggested structure has advantages of simplicity, compact size and high ER with low IL. It is also easy for fabrication and compatible with the standard CMOS fabrication technology. Additionally, the suggested design is more practical compared to that reported in (El Shamy et al. 2017) with long L_D of 23 μm and large ER based on SOS platform. It is worth noting also that the proposed TM-pass polarizer has an operating wavelength of 2 μm in the MIR region which is different than that reported in (Abd-Elkader et al. 2019b) which is working in the NIR region at wavelength of 1.55 μm .”

2 Design consideration

Figure 1 shows 3D and 2D schematic diagrams of the proposed TM-pass polarizer. The suggested structure is designed to support the propagation of TM mode only. A silicon core of width $w_s = 800$ nm is used with refractive index of 3.48. The core is surrounded by two sapphire layers with identical width w_d and refractive index of 1.7377. The two sapphire layers are coated by two symmetric AZO layers with width of w_i and two layers of ZrN with width of w_z . All layers have the same height h_m of 1.0 μm . The two plasmonic materials are added in the x-direction where the surface plasmon mode is coupled with the main component of the TE mode (E_x or H_y). Initially, the sapphire layers have identical width w_d of 80 nm while the widths of the AZO and ZrN layers are equal to $w_i = 70$ nm and $w_z = 60$ nm, respectively.

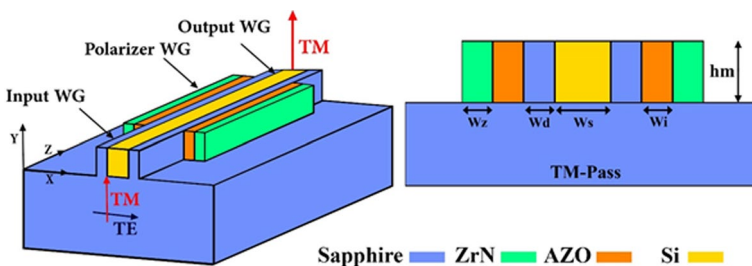


Fig. 1 3D and 2D schematic diagrams of the proposed TM-pass polarizer

Table 1 The Drude-Lorentz model parameters of AZO and ZrN (Naik et al. 2013)

Parameter	AZO	ZrN
ϵ_b	3.5402	3.4656
ω_p	1.7473 eV	8.018 eV
γ_p	0.04486 eV	0.5192 eV
f_1	0.5095	2.4509
ω_1	4.2942 eV	5.48 eV
γ_1	0.1017 eV	1.7369 eV

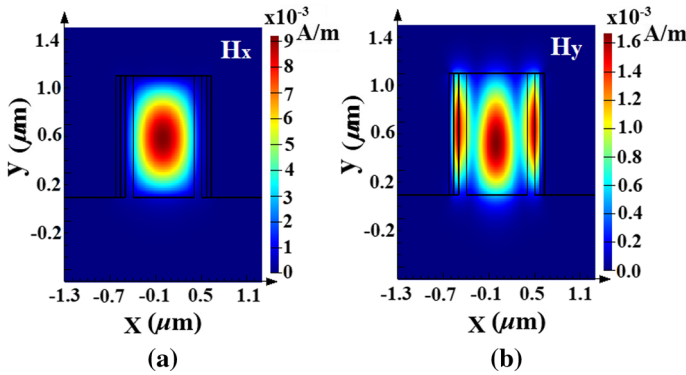


Fig. 2 Field plots of the **a** H_x and **b** H_y of the quasi-TM and quasi-TE modes, respectively

The relative permittivity of the AZO and ZrN at a wavelength of $\lambda=2 \mu\text{m}$ are taken as $-3.8316 + 0.57253i$ and $-92.295 + 82.32i$, respectively. These values are obtained from the following Drude Lorentz model based on the spectroscopic ellipsometry measurements reported in (Naik et al. 2013) over the wavelength range 350–2000 nm without the need for electric biasing.

$$\epsilon(\omega) = \epsilon_b - \frac{\omega_p^2}{\omega(\omega + i\gamma_p)} + \frac{f_1\omega^2}{\omega_1^2 - \omega^2 - i\omega\gamma_1} \tag{1}$$

where the AZO and ZrN parameters are given in Table 1 (Naik, et al. 2013). Figure 2 depicts the magnetic field intensities of the quasi-TM and quasi-TE modes’ main components H_x and H_y , respectively. It can be observed that H_x of the quasi-TM mode has a good confinement through the silicon core. However, H_y of the quasi-TE mode has more leakage toward the plasmonic materials. Thus, high losses occur for the TE mode only.

The TM-pass polarizer has high losses for the TE mode while the TM mode has low attenuation. As a result, our goal is to maximize the figure of merit (FOM) for the suggested polarizer, which is defined as follow (Alam et al. 2012; Kandeel et al. 2019).

$$FOM = \frac{\text{Propagation losses of TE mode} \left(\frac{dB}{\mu\text{m}} \right)}{\text{Propagation losses of TM mode} \left(\frac{dB}{\mu\text{m}} \right)} \tag{2}$$

3 Numerical results

In order to design highly efficient and compact TM-pass polarizer based on SOS platform, the geometrical parameters of the suggested design are studied to maximize the FOM with good polarization filtering characteristics. The modal characteristics of the proposed polarizer are studied using a full-vectorial finite element approach (Obayya et al. 2000, 2002; Rahman et al. 2008) based on COMSOL Multiphysics software package (<https://www.comsol.com>) with a minimum element size of $6 \times 10^{-4} \mu\text{m}$ and a perfect matched layer boundary condition. The propagation characteristics of the proposed polarizer are performed by using 3D finite difference time domain (FDTD) simulations using Lumerical software package (<https://www.lumerical.com>). The FDTD simulations are employed to check the filtering characteristics and calculate the ER of the reported polarizer. The ER can be defined as (Abd-Elkader et al. 2019b).

$$ER(\text{dB}) = 10 \cdot \log \left(\frac{P_{out}^p}{P_{in}^p} \cdot \frac{P_{in}^c}{P_{out}^c} \right) \tag{3}$$

where (P_{out}^p/P_{in}^p) is the ratio of the power at the output terminal to the power at the input of the passed mode. Also, (P_{out}^c/P_{in}^c) is the ratio of the filtered mode’s output power to its input power. Additionally, the insertion loss (IL) is considered as

$$IL(\text{dB}) = 10 \log_{10} \left(\frac{P_{out}^p}{P_{in}^p} \right) \tag{4}$$

where P_{in}^p and P_{out}^p refer to the power of the passed polarization state at the input and the output of the polarizer, respectively. The grid size used for the 3D FDTD is $\Delta x = 10 \text{ nm}$, $\Delta y = 10 \text{ nm}$, $\Delta z = 0.1 \mu\text{m}$.

The effect of the sapphire layers width is first investigated. Figure 3 indicates the ER and FOM dependence on the width of sapphire layers (w_d) at a device length of $3.0 \mu\text{m}$ and an operating wavelength of $2.0 \mu\text{m}$. It can be noticed from Fig. 3a that the ER increases from 3.8 to 20.3 dB as the width of the sapphire layers w_d increases from 60 to 100 nm. Then, the ER decreases to 3.6 dB by increasing w_d to 140 nm. The behavior of the FOM is

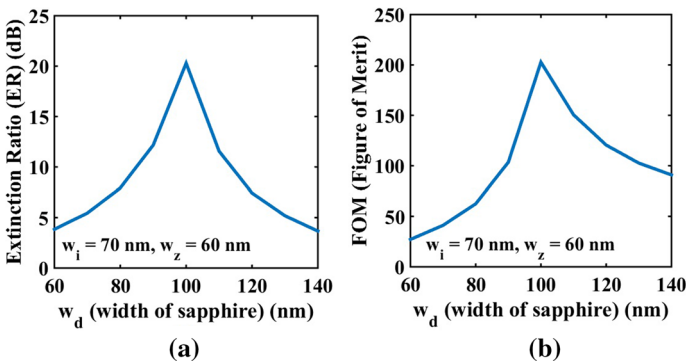


Fig. 3 Variations of **a** ER and, **b** FOM with the width of the sapphire layer (w_d) at $L_D = 3.0 \mu\text{m}$ and $\lambda = 2 \mu\text{m}$. The widths of the AZO and ZrN layers are set as $w_i = 70 \text{ nm}$ and $w_z = 60 \text{ nm}$, respectively

relatively matched with that of the ER as can be seen from Fig. 3b, where ER of 20.3 dB can be achieved at $w_d = 100$ nm. Figure 4 illustrates the variation of the ER and FOM with the widths of the AZO (w_i) and ZrN (w_z) layers at 3.0 μm device length. The ER as a function of the AZO layers width (w_i) at different widths of ZrN (w_z) layers is presented in Fig. 4a, while, the variation of the FOM with the AZO layers width (w_i) at different ZrN (w_z) layers widths is plotted in Fig. 4b. It can be observed that the ER and FOM increase as the width of the AZO layers w_i increase from 30 to 70 nm. If w_i is further increased to 110 nm the ER and FOM decrease for the different widths of ZrN (w_z) layers. In can be also seen from Fig. 4a and b that w_z has a slight effect on the ER and FOM. In order to investigate that effect, the dependence of field distribution $|E_x|$ of the filtered TE mode on the widths of ZrN (w_z) layers is presented in Fig. 4c. It is evident from Fig. 4c that such small effect is due to the amount of the field that penetrates the ZrN layer is very small and is independent on the width of the ZrN layers. The ER and FOM have their maximum values of 20.3 dB and 202.8, respectively, at $w_i = 70$ nm and $w_z = 60$ nm.

Figure 5 shows the ER and IL variations with the device length without and with input (i/p) and output (o/p) waveguides. It can be observed from Fig. 5 that the ER and IL rise as the device length of the polarizer increases. Figure 5a shows the effect of the device length on the ER and IL without the existence of input and output waveguides, where, at a

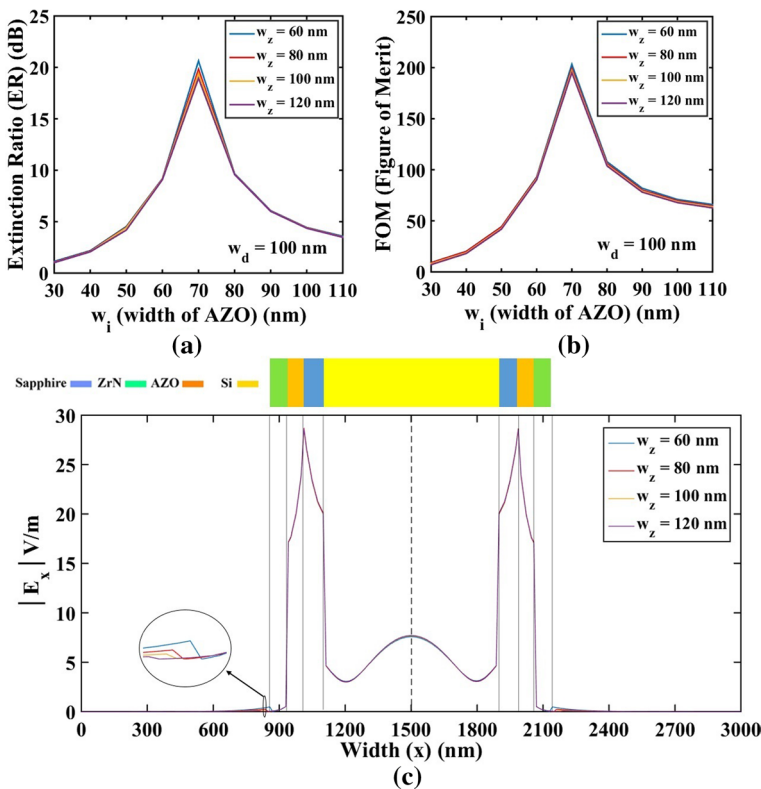


Fig. 4 Dependence of the **a** ER, and **b** FOM on the widths of the AZO (w_i) and the ZrN (w_z) layers at $L_D = 3.0 \mu\text{m}$ and $\lambda = 2 \mu\text{m}$ with the width of the sapphire layers $w_d = 100$ nm. **c** Dependence of the field distribution $|E_x|$ of the filtered TE mode on the widths of the ZrN (w_z) layers at $w_i = 70$ nm and $w_d = 100$ nm

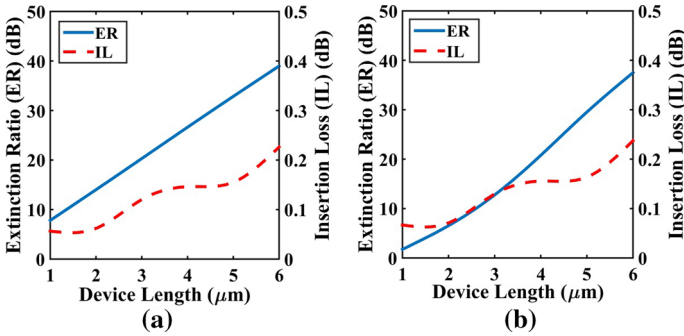


Fig. 5 The dependence of the ER and IL on the device length at $\lambda=2 \mu\text{m}$ **a** without input and output waveguides and **b** with input and output waveguides. The widths of the sapphire, AZO and ZrN layers are set as $w_d=100 \text{ nm}$, $w_i=70 \text{ nm}$ and $w_z=60 \text{ nm}$, respectively

compact L_D of $3.0 \mu\text{m}$ and $\lambda=2.0 \mu\text{m}$, the proposed TM-pass polarizer has $\text{ER}=20.3 \text{ dB}$ and $\text{IL}=0.14 \text{ dB}$. In order to mimic the reality, where the input power is launched by an input laser source to excite the fundamental modes to propagate through the proposed TM-pass polarizer, a study is performed to investigate the effect of the device length on the ER and IL with the presence of i/p and o/p waveguides. The input and output waveguides are SOS waveguides without AZO and ZrN layers as shown in Fig. 1. In this case, the ER and IL are equal to 12.6 dB and 0.15 dB , respectively, at a polarizer length of $3.0 \mu\text{m}$ and $0.2 \mu\text{m}$ input and output waveguide lengths. The resultant decrease in the ER and the rise in the IL are owing to the coupling loss at the interfaces between the i/p and o/p waveguides and the polarizer. The ripples shown in Fig. 5 are due to the Fabry–Perot cavity effect between the two end faces of the polarizer waveguide (Abd-Elkader et al. 2019b). From the numerical analysis, the optimum dimensions of the suggested TM-pass polarizer are summarized in Table 2.

The light propagation of the two polarized modes through the whole structure (the polarizer with both input and output waveguides is shown in Fig. 6. It may be seen from Fig. 6a that the TM mode propagates with low losses through the reported design. However, the TE mode does not propagate and suffers from high attenuation as shown in Fig. 6b.

In order to clarify the importance of using bimetallic configuration in the suggested design, the following comparison has been made. In this study, the effect of using AZO or ZrN alone on the extinction ratio (ER) and insertion loss (IL) are investigated and compared to that obtained using the bimetallic configuration. Figure 7a shows the field distribution

Table 2 Optimum geometry of the TM-pass polarizer

Parameter	Value
h_m	1000 nm
w_s	800 nm
w_d	100 nm
w_i	70 nm
w_z	60 nm
Device length	3 μm

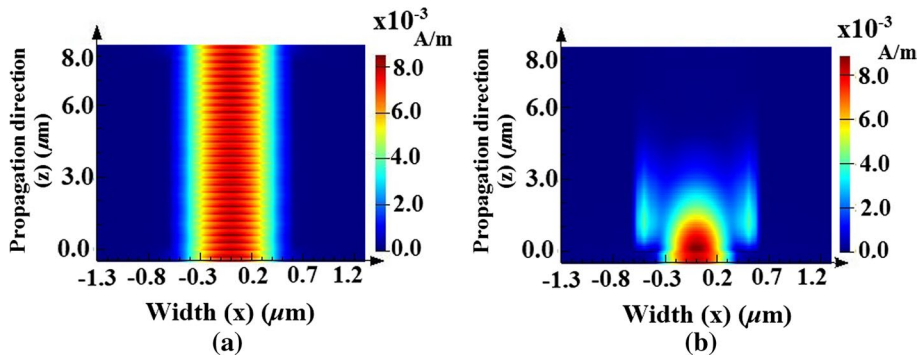


Fig. 6 Field evolution through the suggested TM-pass polarizer with input and output waveguides excited by the quasi **a** TM and, **b** TE input modes. The widths of the sapphire, AZO and ZrN layers are set as $w_d=100$ nm, $w_i=70$ nm and $w_z=60$ nm, respectively

$|E_x|$ of the filtered TE mode due to the bimetallic design with width of 130 nm and compared to that obtained using AZO only with different layer widths. It can be seen from the figure that the bimetallic case ($w_i(\text{AZO})=70$ nm, $w_z(\text{ZrN})=60$ nm) has larger amount of field penetration to the AZO/ZrN through the Si core and the Sapphire material. Therefore, the field is highly attenuated by the plasmonic materials which is highly needed for filtering process. Whereas in the case of using AZO only, most of the field is confined in the Si core and only a small amount is passed to the plasmonic materials. therefore the filtration process is very weak by using AZO only. Further, Fig. 7b and c show that low ER is achieved using device length range from 1 to 6 μm based on AZO only with width range from 70 to 170 nm. At a device length of 3 μm , the ER is always less than 4 dB while an ER = 20.3 dB is obtained when using AZO and ZrN materials. It is also observed that, at device length of 3 μm , the IL = 0.14 dB for the bimetallic configuration while the use of AZO alone produces minimum IL of 0.07 dB.

Figure 8 shows a comparison between the performances of the suggested design with bimetallic configuration with that obtained using ZrN only. Figure 8a explores the field distribution $|E_x|$ of the filtered TE mode due to the AZO/ ZrN with total thickness of 130 nm and that obtained using ZrN only with different layer widths. It can be noticed from the figure that the use of ZrN only results in very small amount of field penetration through the plasmonic material with a good confinement in the Si/sapphire layers. Therefore, the TE filter performance is weak. However, the bimetallic configuration has a good field penetration to the plasmonic materials which attenuates well the TE mode. This is evident in Fig. 8b and c where the use of ZrN only has ER < 0.1 dB with minimum IL of 0.34 dB at a device length of 3 μm .

The fabrication tolerance of the different geometrical parameters is then investigated. The thickness of the sapphire, AZO and ZrN layers are studied with a tolerance of ± 10 nm around the optimum values. Figure 9 illustrates the dependence of the ER and IL on the widths (w_i) of AZO layer and w_z of ZrN layer. It can be observed from Fig. 9a that the polarizer has a tolerable performance over the entire range of w_i variations at $w_d=100$ nm and $w_z=60$ nm, where the ER is always greater than 10 dB for the w_i range from 61 to 79 nm with IL < 0.15 dB. On the other hand, Fig. 9b demonstrates how the tolerance of the ZrN layer width w_z while w_d and w_i remain constant at 100 nm and 70 nm, respectively. It can be seen that the ER is always greater than 20 dB while the IL is less than 0.142 dB.

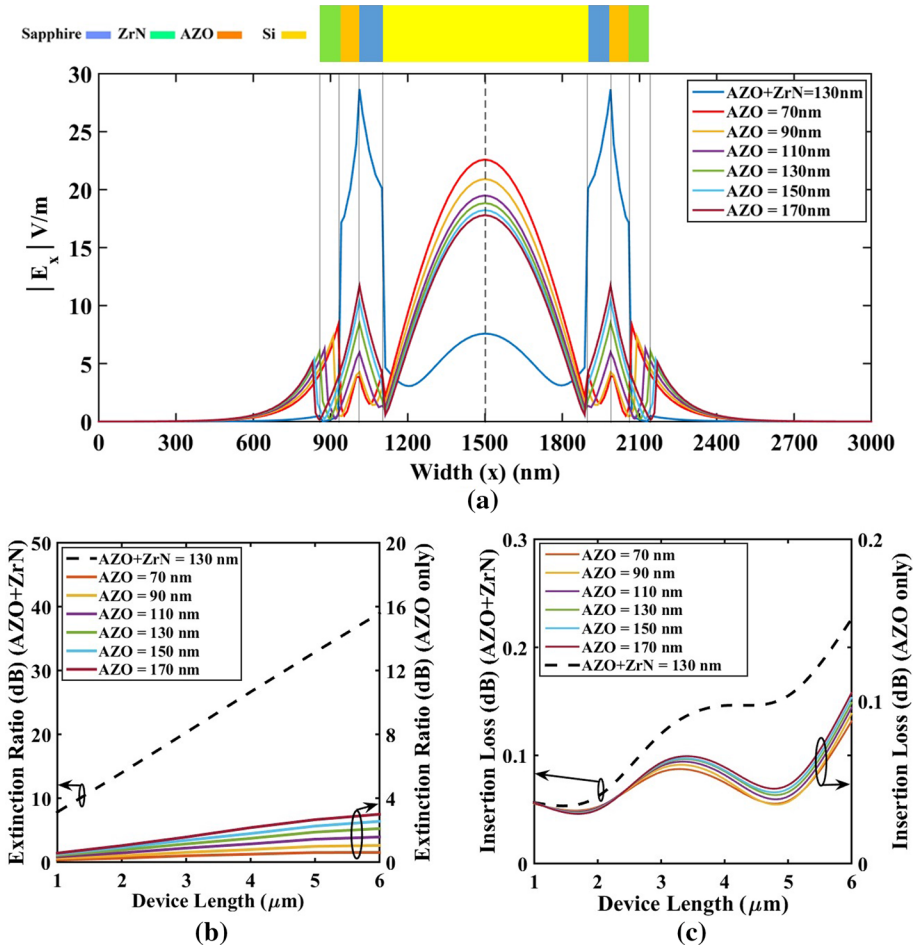


Fig. 7 The impact of the plasmonic layers, for (AZO+ZrN) Vs. (AZO only) on **a** the field distribution $|E_x|$ of the filtered TE mode, **b** ER, and **c** IL at different device lengths at an operating wavelength of 2 μm with the width of the sapphire layers $w_d = 100$ nm

The fabrication tolerance of the sapphire layer width w_d is then investigated. Figure 10 illustrates the impact of the width w_d of the sapphire layer on the ER and IL. However, the other geometries are constant at $w_i = 70$ nm, and $w_z = 60$ nm. It can be seen that the IL is always less than 0.16 dB with ER better than 12 dB over the studied range. Therefore, the suggested TM-pass polarizer has a good tolerance to fabrication imperfections.

The proposed polarizer's performance with the operating wavelength variation is also investigated as shown in Fig. 11. It is revealed from this figure that the presented TM-pass polarizer achieves ER higher than 20.3 dB over a wavelength range of 1.94:2.06 μm with IL less than 0.16 dB.

The suggested design can be fabricated using the current technology. The silicon core can be implemented using electron beam lithography. However, thermal oxidation (Gusev et al. 1995) can be used to define the sapphire layer. Further, the CVD or sputtering can be utilized to deposit the plasmonic layers (Hess and Graves 1993).

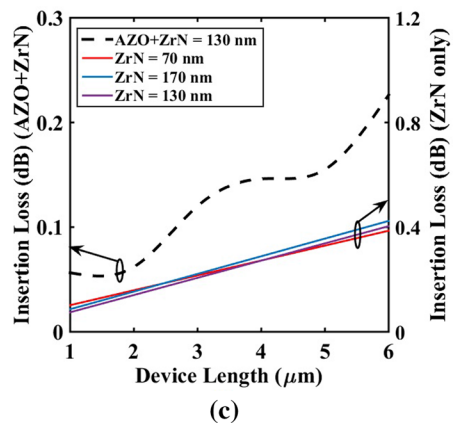
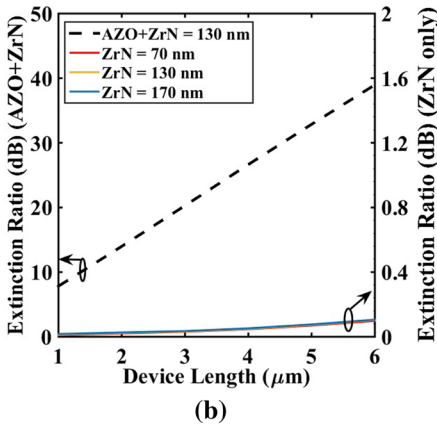
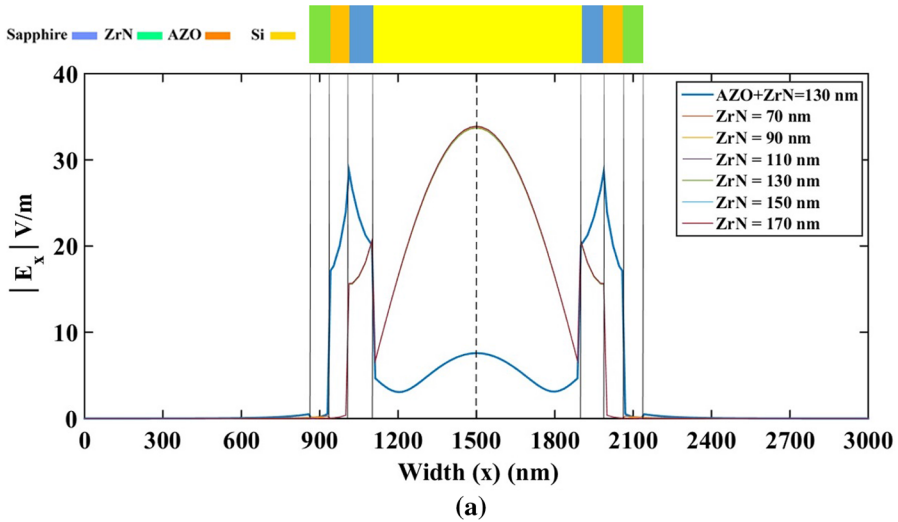


Fig. 8 The impact of the plasmonic layers, for (AZO + ZrN) Vs. (ZrN only) on **a** the field distribution $|E_x|$ of the filtered TE mode, **b** ER, and **c** IL at different device lengths at an operating wavelength of $2 \mu\text{m}$ with the width of the sapphire layers $w_d = 100 \text{ nm}$

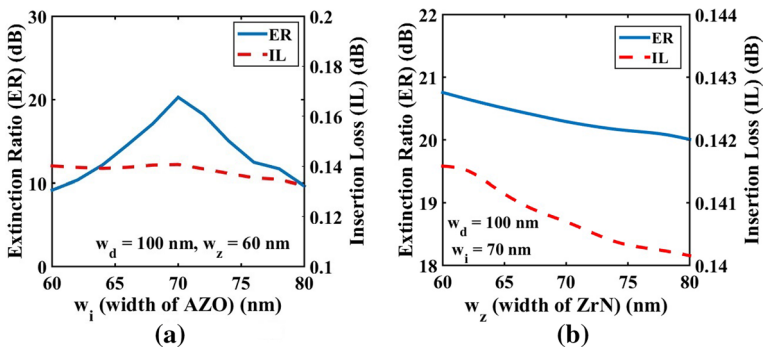


Fig. 9 Effect of widths variations of the **a** AZO and **b** ZrN layers on the extinction ratio and insertion loss for the TM-pass polarizer at $L_D = 3.0 \mu\text{m}$ and $\lambda = 2 \mu\text{m}$ with the width of the sapphire layers $w_d = 100 \text{ nm}$

Fig. 10 Effect of the width w_d of the sapphire layer on the extinction ratio and insertion loss at $L_D = 3.0 \mu\text{m}$ and $\lambda = 2 \mu\text{m}$ with the widths of the AZO and ZrN layers are set as $w_i = 70 \text{ nm}$ and $w_z = 60 \text{ nm}$, respectively

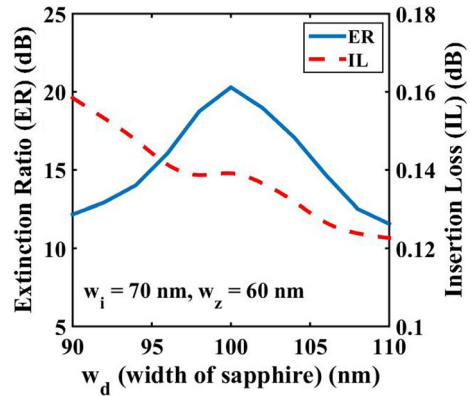


Fig. 11 The wavelength dependent extinction ratio and insertion loss at $L_D = 3.0 \mu\text{m}$. The widths of the sapphire, AZO and ZrN layers are taken as $w_d = 100 \text{ nm}$, $w_i = 70 \text{ nm}$ and $w_z = 60 \text{ nm}$, respectively

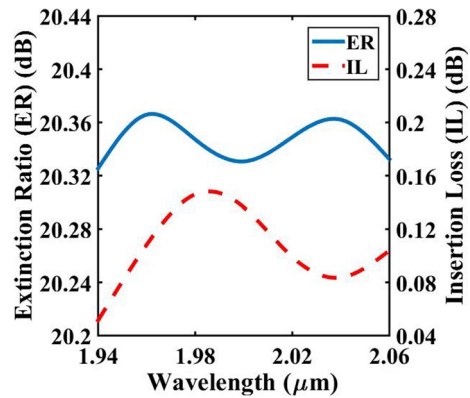


Table 3 illustrates a comparison between the proposed structure and those reported in the literature in terms of the device length, ER, IL, CMOS compatibility, used platform, wavelength range, and type of work (theoretical or experimental). The MIR operation is the most important feature of the proposed TM-pass polarizer based on the SOS platform. It may be seen that most of the polarizers in the literature are dependent on the SOI platform. Additionally, the suggested design has a shorter device length than that reported in Wang and Ho (2010), Guan et al. (2014), El Shamy et al. (2017), Alam et al. (2011), and Ng et al., (2012). It has also a higher ER than that reported in Azzam and Obayya (2015), and Azzam and Obayya, (2016). Moreover, it achieves a lower IL than that proposed in Guan et al., (2014), (Kandeel et al. 2019), Azzam et al., (2014), El Shamy et al. (2017), Alam et al. (2011), Bai et al., (2017), and Azzam and Obayya (2016).

4 Conclusion

TM-pass polarizer based on SOS platform is introduced and analyzed for MIR application. The suggested polarizer has bi-metallic configuration of AZO and ZrN materials at a wavelength of $2.0 \mu\text{m}$. The reported design achieves high ER of 20.3 dB with low IL of 0.14 dB at a device length of $3.0 \mu\text{m}$. The proposed polarizer is compatible with current

Table 3 Comparison of the suggested design to those reported in the literature

Design	Length (μm)	ER (dB)	IL (dB)	CMOS compat- ibility	Platform	Wavelength range	Experimental or numerical
This work	3	20.3	0.14	Yes	SOS	(MIR) 2 μm	Numerical
(El Shamy et al. 2017)	23	69.77	1.21	Yes	SOS	(MIR) [2–6] μm	Numerical
(Kandeel et al. 2019)	2	31.5	0.17	Yes	SOI	(NIR) 1.55 μm	Numerical
(Wang and Ho 2010)	10	26	–	Yes	SOI	(NIR) 1.55 μm	Numerical
(Guan et al. 2014)	9	27	0.5	Yes	SOI	(NIR) 1.55 μm	Experimental
(Azzam et al. 2014)	2.5	30	0.4	Yes	SOI	(NIR) [1.45–1.68] μm	Numerical
(Azzam and Obayya 2015)	1.3	20	0.15	Yes	SOI	(NIR) 1.55 μm	Numerical
(Alam et al. 2011)	10	–	3	No	SOI	(NIR) 1.55 μm	Numerical
(Bai et al. 2017)	2.5	25	0.088	No	SOI	(NIR) 1.55 μm	Numerical
(Saber et al. 2018)	15	30.11	3.08	Yes	SOI	(NIR) [1.5–1.6] μm	Numerical
(Azzam and Obayya 2016)	2.48	20	0.96	Yes	SOI	(NIR) 1.55 μm	Numerical
(Abd-Elkader et al. 2019b)	1	22	0.11	Yes	SOI	(NIR) 1.55 μm	Numerical

CMOS fabrication procedures and provides acceptable performance over a wide range of bandwidths with high resistant to fabrication errors.

Funding Open access funding provided by The Science, Technology & Innovation Funding Authority (STDF) in cooperation with The Egyptian Knowledge Bank (EKB).

Declarations

Conflict of interest The authors declare no conflicts of interest.

Open Access This article is licensed under a Creative Commons Attribution 4.0 International License, which permits use, sharing, adaptation, distribution and reproduction in any medium or format, as long as you give appropriate credit to the original author(s) and the source, provide a link to the Creative Commons licence, and indicate if changes were made. The images or other third party material in this article are included in the article's Creative Commons licence, unless indicated otherwise in a credit line to the material. If material is not included in the article's Creative Commons licence and your intended use is not permitted by statutory regulation or exceeds the permitted use, you will need to obtain permission directly from the copyright holder. To view a copy of this licence, visit <http://creativecommons.org/licenses/by/4.0/>.

References

- Abd-Elkader, A.E.S., Hameed, M.F.O., Areed, N.F., Mostafa, H.E.D., Obayya, S.S.A.: Highly tunable compact polarization rotator based on silicon on insulator platform. *Opt. Quant. Electron.* **51**(5), 1–18 (2019a)
- Abd-Elkader, A.E.S., Hameed, M.F.O., Areed, N.F., Mostafa, H.E.D., Obayya, S.S.A.: Ultracompact AZO-based TE-pass and TM-pass hybrid plasmonic polarizers. *J. Opt. Soc. Am. B* **36**(3), 652–661 (2019b)
- Alam, M., Aitchison, J.S., Mojahedi, M.: Compact hybrid TM-pass polarizer for silicon-on-insulator platform. *Appl. Opt.* **50**(15), 2294–2298 (2011)
- Alam, M., Aitchison, J.S., Mojahedi, M.: Compact and silicon on- insulator-compatible hybrid plasmonic TE-pass polarizer. *Opt. Lett.* **37**(1), 55–57 (2012)
- Azzam, S.I.H., Hameed, M.F.O., Areed, N.F., Abd-Elrazzak, M.M., El-Mikati, H., Obayya, S.S.A.: Proposal of an ultracompact CMOS-compatible TE-/TM-pass polarizer based on SoI platform. *IEEE Photon. Technol. Lett.* **26**(16), 1633–1636 (2014)
- Azzam, S.I., Obayya, S.S.A.: Ultra-compact resonant tunneling-based TE-pass and TM-pass polarizers for SOI platform. *Opt. Lett.* **40**(6), 1061–1064 (2015)
- Azzam, S.I., Obayya, S.S.A.: Titanium nitride-based CMOS-compatible TE-pass and TM-pass plasmonic polarizers. *IEEE Photon. Technol. Lett.* **28**(3), 367–370 (2016)
- Bai, B., Liu, L., Chen, R., Zhou, Z.: Low loss, compact TM-pass polarizer based on hybrid plasmonic grating. *IEEE Photon. Technol. Lett.* **29**(7), 607–610 (2017)
- COMSOL 5.1 Multiphysics software, <https://www.comsol.com>
- El Shamy, R.S., Mossad, H., Swillam, M.A.: Silicon-on-sapphire (SOS) waveguide modal analysis for mid-infrared applications. *J. Phys. Comm.* **1**(3), 35011-1–35011-13 (2017)
- Guan, X., Chen, P., Chen, S., Xu, P., Shi, Y., Dai, D.: Low-loss ultracompact transverse-magnetic-pass polarizer with a silicon subwavelength grating waveguide. *Opt. Lett.* **39**(15), 4514–4517 (2014)
- Gusev, E.P., Lu, H.C., Gustafson, T., Garfunkel, E.: Growth mechanism of thin silicon oxide films on Si (100) studied by medium-energy ion scattering. *Phys. Rev. B* **52**(3), 1759–1775 (1995)
- Hameed, M.F.O., Obayya, S.S.A.: Polarization rotator based on soft glass photonic crystal fiber with liquid crystal core. *J. Lightw. Technol.* **29**(18), 2725–2731 (2011)
- Hameed, M.F.O., Obayya, S.S.A.: Ultrashort silica liquid crystal photonic crystal fiber polarization rotator. *Opt. Lett.* **39**(4), 1077–1080 (2014)
- Hess, W., Graves, D.B.: Plasma assisted chemical vapor deposition. In: Hitchman, M.L., Jensen, K.F. (eds.) *Chemical vapor deposition: principles and applications*, pp. 385–435. Academic Press Ltd, San Diego (1993)
- Kandeel, A.F., Hameed, M.F.O., AbdElHamid, H., Obayya, S.S.A.: CMOS-compatible hybrid bi-metallic TE/TM-pass polarizers based on ITO and ZrN. *Appl. Opt.* **58**(24), 6684–6692 (2019)

- Lin, J.Y., Zhong, K.D., Lee, P.T.: Plasmonic behaviors of metallic AZO thin film and AZO nanodisk array. *Opt. Expr.* **24**(5), 5125–5135 (2016)
- Lloyd, J.M.: *Thermal Imaging Systems*. Springer Science & Business Media, New York (2013)
- Lumerical FDTD Solutions Software, <https://www.lumerical.com/tcad-products/fdtd/>
- Mueller, C.W., Robinson, P.H.: Grown-film silicon transistors on sapphire. *Proc. IEEE* **52**(12), 1487–1490 (1964)
- Naik, G.V., Kim, J., Boltasseva, A.: Oxides and nitrides as alternative plasmonic materials in the optical range. *Opt. Mater. Expr.* **1**(6), 1090–1099 (2011)
- Naik, G.V., Shalaev, V.M., Boltasseva, A.: Alternative plasmonic materials: beyond gold and silver. *Adv. Mater.* **5**(24), 3264–3294 (2013)
- Ng, T.K., Khan, M.Z.M., Al-Jabr, A., Ooi, B.S.: Analysis of CMOS compatible Cu-based TM-pass optical polarizer. *IEEE Photon. Technol. Lett.* **24**(9), 724–726 (2012)
- Obayya, S.S.A., Rahman, B.M.A., El Mikati, H.A.: New full vectorial numerically efficient propagation algorithm based on the finite element method. *J. Lightw. Technol.* **18**(3), 409–415 (2000)
- Obayya, S.S.A., Rahman, B.M.A., Grattan, K.T.V., El Mikati, H.A.: Full vectorial finite-element-based imaginary distance beam propagation solution of complex modes in optical waveguides. *J. Lightw. Technol.* **20**(6), 1054–1060 (2002)
- Rahman, B.M.A., Leung, D.M.H., Obayya, S.S.A., Grattan, K.T.V.: Numerical analysis of bent waveguides: bending loss, transmission loss, mode coupling, and polarization coupling. *Appl. Opt.* **47**(16), 2961–2970 (2008)
- Saber, M.G., Abadía, N., Plant, D.V.: CMOS compatible all-silicon TM pass polarizer based on highly doped silicon waveguide. *Opt. Expr.* **26**(16), 20878–20887 (2018)
- Schliesser, A., Picqué, N., Hänsch, T.W.: Mid-infrared frequency combs. *Nat. Photon.* **6**(7), 440–449 (2012)
- Soref, R., Lorenzo, J.: All-silicon active and passive guided-wave components for $\lambda = 1.3$ and $1.6 \mu\text{m}$. *IEEE J. Quant. Electron.* **22**(6), 873–879 (1986)
- Swillam, M.A., El Shamy, R.S., Gan, Q., Khalil, D.: Mid-infrared plasmonic gas sensor. *Photon. Phonon. Prop. Eng. Nanostruct.* **10541**, 105411O-1–105411O-8 (2018). <https://doi.org/10.1117/12.2290875>
- Wang, Q., Ho, S.-T.: Ultracompact TM-pass silicon nanophotonic waveguide polarizer and design. *IEEE Photon. J.* **2**(1), 49–56 (2010)
- Zou, Y., Chakravarty, S., Chung, C.J., Xu, X., Chen, R.T.: Mid-infrared silicon photonic waveguides and devices. *Photon. Res.* **6**(4), 254–276 (2018)

Publisher's Note Springer Nature remains neutral with regard to jurisdictional claims in published maps and institutional affiliations.